Rev.Adv.Mater.Sci. 18(2008) 454-458

EARLY STAGES OF PHASE SEPARATION AND NANOCRYSTALLIZATION IN Al-RARE EARTH METALLIC GLASSES STUDIED USING SAXS/WAXS AND HRTEM METHODS

Jerzy Antonowicz[1], Elzbieta Jezierska[2], Marcin Kędzierski[1], Alain Reza Yavari[3], Lindsay Greer[4], Pierre Panine[5] and Michael Sztucki[5]

[1]Faculty of Physics, Warsaw University of Technology, Koszykowa 75, 00-662 Warsaw, Poland
[2]Faculty of Materials Science and Engineering, Warsaw University of Technology, Woloska 141, 02-507 Warsaw, Poland
[3]Institut National Polytechnique de Grenoble, (LTPCM-CNRS umr 5614),1130 Rue de la Piscine, BP 75, 38402 St-Martin-d'Heres Campus, France
[4]Department of Materials Science and Metallurgy, University of Cambridge, Pembroke Street, Cambridge CB2 3QZ, U.K.
[5]European Synchrotron Radiation Facility, 6 rue Jules Horowitz, BP220, 38043 Grenoble Cedex, France

Received: March 29, 2008

Abstract. Early stages of nanocrystallization in $Al_{92}Sm_8$ and $Al_{91}Gd_9$ glassy melt-spun alloys were investigated *in-situ* using simultaneous small- and wide-angle X-ray scattering (SAXS/WAXS). The measurements were performed during isothermal annealing at temperatures below crystallization point. The results are supported by high resolution transmission electron microscopy (HRTEM). In both alloys a continuous SAXS signal increase was observed during annealing while WAXS revealed fully amorphous structure. After the initial transient, the Bragg peaks of the fcc-Al nanocrystalline phase start to appear on the "halo" diffraction pattern. HRTEM images of the annealed samples show presence of nanometer-size crystalline grains embedded in the amorphous matrix. Within the experimental conditions a minimal detectable crystalline volume fraction was estimated to be 0.05%. The results indicate that amorphous phase separation prior to crystallization occurs in investigated systems. A presence of a characteristic signal maximum in a small-angle region suggests that glassy phase separation proceeds by a spinodal mechanism. It is concluded that nanocrystallization in aluminium-rare earth metallic glasses is triggered and controlled by the phase separation process.

1. INTRODUCTION

During last years nanocrystallization in aluminium-based metallic glasses containing rare earth (RE) or rare earth and transition metals additions was a subject of intensive studies. Despite of that the mechanism underlying formation of ultra fine microstructure is still not fully recognized and attracts significant attention.

Al-based amorphous alloys (for a review, see [1]) posses attractive mechanical properties like high strength and good ductility. Thermal treatment of some of these alloys leads to devitrification via formation of fine fcc-Al crystals with average size of about 10 nm and of a density of about 10^{22} - 10^{23} m^{-3} embedded in an amorphous matrix. Such nanocomposites have significantly better mechani-

Corresponding author: Jerzy Antonowicz, e-mail: antonowi@if.pw.edu.pl

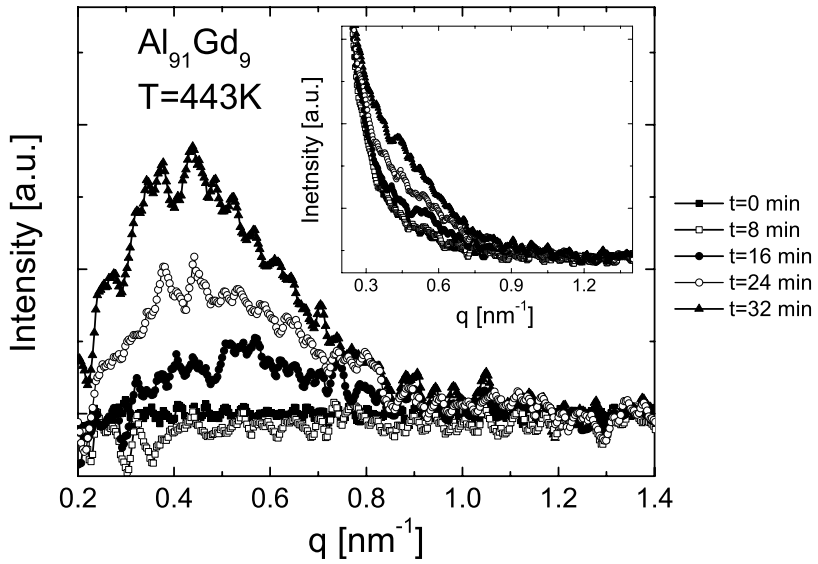

Fig. 1. SAXS spectra development during initial 32 min of annealing of $Al_{91}Gd_9$ alloy at 443K. The inset shows the data without subtraction of the constant signal contribution ascribed to scattering from sample's surface imperfections.

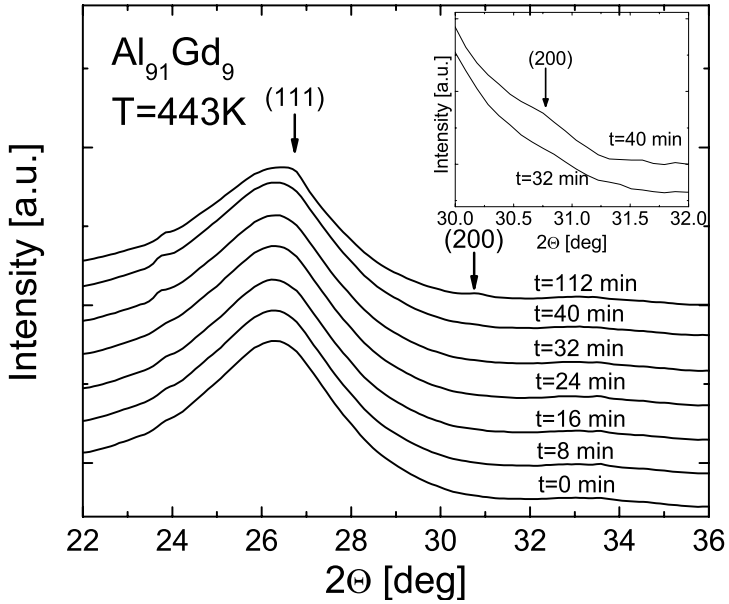

Fig. 2. Changes in WAXS spectra during annealing of $Al_{91}Gd_9$ alloy at 443K. The arrows indicate the positions of (111) and (200) peaks of the fcc-Al crystalline phase. During initial 32 min of annealing the WAXS spectra exhibit a "halo" pattern indicating fully amorphous character of the sample. The inset shows comparison of enlarged fragments of diffraction spectra acquired after 32 min and 40 min of annealing.

cal properties than their glassy precursors. The mechanisms that lead to the extremely high nucleation frequency and sluggish growth rate, required for nanocrystallization, are poorly understood. Nanocrystallization of the Al-based glasses was ascribed to heterogeneous nucleation [2], "quenchedin" nuclei [3,4] and a new type of homogeneous nucleation5. Most recently, data suggesting occurrence of amorphous phase separation were reported [6-9].

This work is an extension of our recent studies focused on determining the mechanism of nanocrystal formation in binary Al-RE rapidly quenched amorphous alloys using SAXS/WAXS

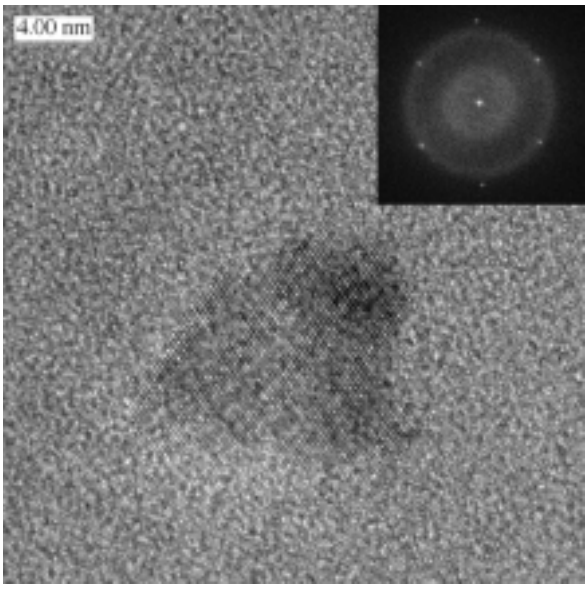

Fig. 3. HRTEM image of a fcc-Al nanocrystal formed in initially amorphous $Al_{91}Gd_9$ alloy annealed isochronically up to 455K at 10 K/min heating rate. The inset shows fast Fourier transform of the image.

method. Our previous results [8,9] suggest that nanocrystallization in Al-RE glasses is a complex process where fine-scale amorphous phase separation triggers crystal nucleation and restricts grain growth. The main objective of this work was to investigate the early stages of phase separation and nanocrystallization. In order to accomplish this task the measurements were carried out *in-situ* during isothermal annealing at temperatures below the crystallization point determined from the calorimetric data. At these temperatures the transformation kinetics was slow enough for observation of the initial stages of the process. The SAXS/WAXS results are supported by high-resolution transmission electron microscopy (HRTEM) data.

2. EXPERIMENTAL

Ingots of $Al_{92}Sm_8$ and $Al_{91}Gd_9$ alloys were prepared using an arc-melting furnace. Amorphous ribbons were produced in a single-roller melt-spinning device operating at wheel speed of 33 m/s. Thus prepared ribbons were about 25 mm thick and about 2 mm wide. The SAXS/WAXS measurements were performed at ID02 beamline of the European Synchrotron Radiation Facility. The small pieces of as-quenched ribbons were sealed in glassy capillaries under argon atmosphere. Samples were placed in a *Linkam* hot-stage allowing sample temperature control with precision of 1K. The isothermal annealing temperature was reached at 90 K/min heating rate. The incident beam wavelength λ = 1.00 Å was used. The SAXS q-range covered 0.07 - 1.85 nm^{-1} ($q = (4\pi/\lambda)\sin\theta$, where θ is half the scattering angle) and WAXS measurements covered 4 - 44 deg of 2θ range. Both SAXS and WAXS spectra were acquired by two-dimensional (2-D) CCD cameras. The 2-D images were processed online to obtain final 1-D spectra. The details of the image processing are available in [10]. In order to achieve similar sensitivity of both methods, the gain levels of SAXS and WAXS detectors were kept approximately equal during whole experiment. The spectra were collected every 60 s with acquisition time of 1 s. The TEM/HRTEM specimens were prepared using electrochemical polishing method and analyzed in a Joel 3010 microscope operating at 300 kV.

3. RESULTS AND DISCUSSION

The samples were annealed at temperatures below their crystallization onset points evaluated from Differential Scanning Calorimetry (DSC) isochronal runs. Thus determined crystallization temperatures were equal 438K and 450K for $Al_{92}Sm_8$ and $Al_{91}Gd_9$ alloys respectively. Fig. 1 presents changes of the small-angle spectra during initial 32 min of annealing of $Al_{91}Gd_9$ alloy at 443K. The constant signal contribution significant at low q and ascribed to scattering from sample's surface imperfections was subtracted from the spectra. The inset in Fig. 1 shows the data without subtraction. For the sake of clarity only every eight spectra were plotted. During initial 8 min since reaching the target temperature no changes in SAXS spectra are observed. After 16 min of annealing a broad maximum centered approximately at q = 0.56 nm^{-1} begins do develop. The SAXS peak grows with time and it's position shifts towards lower q values.

Simultaneously taken WAXS spectra are shown in Fig. 2. It can be seen that during initial 32 min of annealing the WAXS spectra exhibit a "halo" pattern. A trace of diffraction peak at about 24 deg origins from a single spot on a 2-D WAXS camera image and is probably due to a single, micrometer-size crystal present in the scattering volume. The arrows in Fig. 2 indicate the positions of (111) and (200) peaks of the fcc-Al crystalline phase. When discussing the amorphous character of the

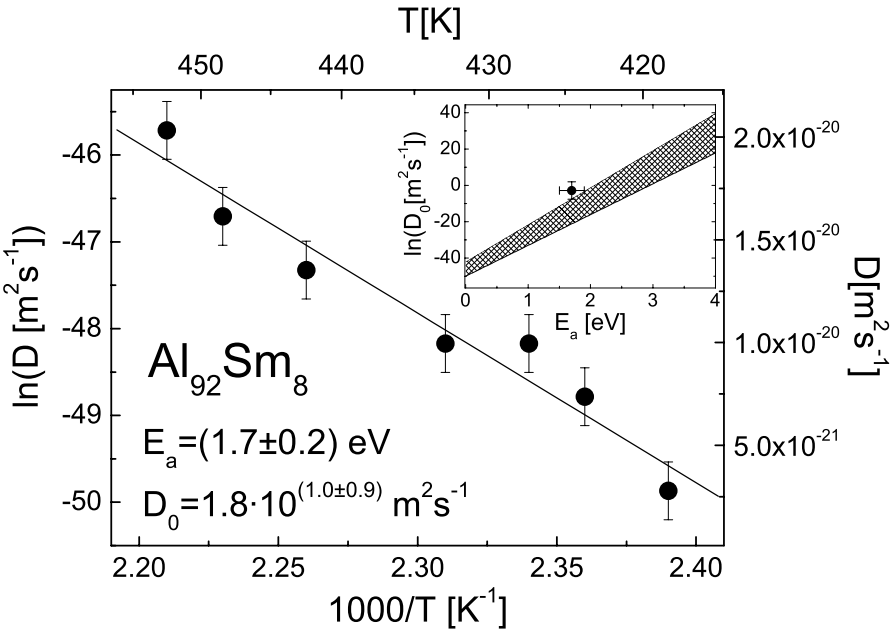

Fig. 4. ln*D* versus 1/*T* plot for $Al_{92}Sm_8$ (circles). The solid line is the linear fit to the experimental points. Values of E_a and D_0 were obtained from the fit parameters. The inset shows experimentally derived correlation between D_0 and E_a for amorphous alloys (taken from [17]) together with the result of this work (full circle).

sample the sensitivity of the method becomes essential. Within the experimental conditions we estimated the minimal detectable amount of crystallinity to be 0.05%. This limit was obtained basing on the recently proposed crystalline volume fraction calculation method [11] and is similar to values obtained in previous experiment [12]. The first traces of the fcc-Al Bragg peaks appear after 40 min of annealing. The inset in Fig. 2 shows comparison of enlarged fragments of diffraction spectra acquired after 32 min and 40 min of annealing. After 32 min no detectible crystallinity is found, while after 40 min a weak (200) Bragg reflex of fcc-Al phase is visible and the crystalline volume fraction reaches the detectability threshold of 0.05%. During further annealing the Bragg peaks of the nanocrystalline phase become more pronounced as demonstrated in Fig. 2. Similar results to those presented above were also obtained for $Al_{92}Sm_8$ amorphous alloy.

In order to investigate the morphology of the crystalline precipitated the preannealed samples were analyzed using HRTEM method. Fig. 3 presents the HRTEM image of a typical fcc-Al nanocrystal formed in initially amorphous $Al_{91}Gd_9$ alloy annealed isochronically up to 455K at 10 K/min heating rate. The inset shows fast Fourier transform of the image. The nanocrystal visible in the image has size of about 14 nm and it's shape is roughly spherical.

The results presented above suggest that compositional fluctuations appear in amorphous Al-RE alloys during annealing prior to the onset of crystallization. A characteristic peak-shaped SAXS signal provides a clear evidence of well defined correlation length even in the initial stages of the transformation. The regular spatial arrangement of fluctuations is a characteristic feature of transformations initiated by spinodal decomposition. Our previous results [8] showed that early stages of SAXS spectra evolution can be successfully analyzed in a framework of Cahn's linear theory of spinodal decomposition [13]. According to this theory the SAXS intensity for given q grows exponentially with time: $I(q) \propto |c\text{-}c_0|^2 \propto \exp(2R(q)t)$, where $c\text{-}c_0$ is the deviation from the homogeneous concentration c_0, $R(q)$ is the q-dependent concentration fluctuation growth rate and t is time. The modulus of a negative interdiffusion coefficient ($D = |\tilde{D}|$) is related to growth rate $R(q)$ by: $R(q)/q^2 = D[1 - q^2/(2q^2_m)]$, where

q_m is the initial position of the SAXS intensity maximum [14]. The value of D can be therefore obtained from the straight line fit of the "Cahn plot" $R(q)/q^2$ vs q^2. According to the linear theory of spinodal decomposition the "Cahn plot" is a straight line, however its' typically observed shape is not linear [15]. Usually the experimental data are analyzed by looking at the tangents at the peak position q_m [16]. The SAXS data for $Al_{92}Sm_8$ alloy were analyzed to obtain Cahn plots for six annealing temperatures ranging from 418 to 448K. In a considered temperature range the values of q_m were found to be independent on temperature within error of 0.05 nm^{-1} and were assumed to be equal 0.60 nm^{-1}. The interdiffusion coefficients D were evaluated from tangent's y axis intercept. Thus obtained values of D were ranging from $2.2 \cdot 10^{-22}$ m^2s^{-1} at 418K to $5.2 \cdot 10^{-20}$ m^2s^{-1} at 448K. Fig. 4 presents the ln$D$ versus $1/T$ plot for $Al_{92}Sm_8$ alloy. It can be concluded that in considered temperature range the interdiffusion coefficient follows Arrhenius dependence $D = D_0 \exp(-E_a/k_BT)$ where Ea is an activation energy and k_B is Boltzmann constant. From the linear fit parameters the activation energy E_a = 1.7 ± 0.2 eV and $D_0 = 1.8 \cdot 10^{(1.0 \pm 0.9)}$ m^2s^{-1} were obtained. The inset in Fig. 4 shows experimentally derived correlation between D_0 and E_a for amorphous alloys (taken from [17]) together with the result of this present work (full circle).

4. CONCLUSIONS

We conclude that in the early stages of annealing of investigated samples the SAXS signal maximum can not be ascribed to nanocrystals embedded in the glassy matrix but that regular compositional fluctuations present in the amorphous phase are responsible for the increase of intensity scattered in the small-angle regime. The initial fluctuation wavelength is approximately 10 nm. The shift of the SAXS peak position towards origin in q space is attributed to coarsening of the decomposed amorphous regions. After the initial transient the Al-rich nanometer-size amorphous regions become unstable against nucleation of thermodynamically favorable fcc-Al crystalline phase. The size of the region constrains growth of the crystalline grains thus leading to formation of nanocrystalline microstructure. For detailed discussion of late stages of phase separation and nanocrystallization in Al-RE metallic glasses see [8,9]. The obtained parameters of interdiffusion fall into range of experimentally observed in amorphous alloys correlation between D_0 and E_a.

ACKNOWLEDGEMENTS

Jerzy Antonowicz gratefully acknowledges the Faculty of Physics of Warsaw University of Technology and PolishMinistry of Science and Higher Education.

REFERENCES

[1] A. Inoue // *Prog. Mater. Sci.* **43** (1998) 365.
[2] M. Calin and U. Koster // *Mater. Sci. For.* **269-272** (1998) 749.
[3] J. Foley, D. Allen and J. Perepezko // *Scripta Mater.* **35** (1996) 655.
[4] G. Wilde, R.I. Wu and J.H. Perepezko, In: *22nd Risř International Symposium on Materials Science: Science of Metastableand Nanocrystalline Alloys: Structure, Properties and Modelling* (September, 2001), p. 429.
[5] K. F. Kelton // *Phil. Mag. Lett.* **77** (1998) 337.
[6] K.F. Kelton, T.K. Croat, A. K. Gangopadhyay and A. L. Greer // *J. Non-Cryst. Solids* **317** (2003) 71.
[7] Y. Wang, H. Yang, B. Sun, B. Wu, J. Wang and M. S. E. Ma // *Scripta Mater.* **55** (2006) 469.
[8] J. Antonowicz, A.R. Yavari, W.J. Botta and P. Panine // *Phil. Mag. A* **86** (2006) 4235.
[9] J. Antonowicz // *J. Alloys Compd.* **434-435** (2007) 126.
[10] P. Boesecke // *J. Appl. Cryst.* , submitted.
[11] J. Antonowicz, A.R. Yavari and G. Vaughan // *Nanotechnology* **15** (2004) 1038.
[12] P. Panine, V. Urban, P. Boesecke and T. Narayanan // *J. Appl. Cryst.* **36** (2003) 991.
[13] J.W. Cahn // *Acta Metall.* **9** (1961) 795.
[14] E. L. Huston, J.W. Cahn and J.E. Hillard // *Acta Metall.* **14** (1966) 1053.
[15] K. Binder and P. Fratzl, *Phase Transformations in Materials* (Wiley-VCH, Weinheim, 2001).
[16] J. S. Langer, M. Baron and H.D. Miller // *Phys. Rev. A* **11** (1975) 1417.
[17] V. Naundorf, M.-P. Macht, A. S. Bakai and N. Lazarev // *Mater. Sci. Forum* **343-346** (2000) 21.